



**Chip-based platform for dynamic analysis of NK cell
cytolysis mediated by a triplebody**

Journal:	<i>Analyst</i>
Manuscript ID	AN-ART-12-2015-002585.R1
Article Type:	Paper
Date Submitted by the Author:	24-Feb-2016
Complete List of Authors:	Chatzopoulou, Elisavet; Ludwig Maximilians Universität, Fakultät für Physik Roskopf, Claudia; Klinikum der Universität München, 2Division of Hematology and Oncology, Medizinische Klinik und Poliklinik IV Sekhavati, Farzad; Ludwig Maximilians Universität, Fakultät für Physik Braciak, Todd; Klinikum der Universität München, 2Division of Hematology and Oncology, Medizinische Klinik und Poliklinik IV Oduncu, Fuat; Klinikum der Universität München, 2Division of Hematology and Oncology, Medizinische Klinik und Poliklinik IV Fey, Georg; Friedrich-Alexander-University Erlangen-Nürnberg, Department of Biology Rädler, Joachim; Ludwig Maximilians Universität, Fakultät für Physik

1
2
3
4 1 **Chip-based platform for dynamic analysis of NK cell**
5 2 **cytolysis mediated by a triplebody**
6
7 3
8

9 4 Elisavet I. Chatzopoulou¹, Claudia C. Roskopf², Farzad Sekhavati¹,

10 5 Todd A. Braciak², Fuat S. Oduncu², Georg H. Fey³ and Joachim O. Rädler^{1*}
11
12
13
14 6

15
16 7 ¹Faculty of Physics and Graduate School of Quantitative Biosciences (QBM), Ludwig-
17 8 Maximilians-Universität, Munich, Germany

18
19 9 ²Division of Hematology and Oncology, Medizinische Klinik und Poliklinik IV, Klinikum der
20 10 Universität München, Munich, Germany

21
22
23 11 ³Department of Biology, Friedrich-Alexander-University Erlangen-Nürnberg, Erlangen,
24 12 Germany

25
26 13 * Correspondence should be sent to: raedler@lmu.de Phone: 0049-(0)89-2180-2438,
27

28 14 Fax: 0049-(0)2180-3182
29
30
31 15
32
33
34

35 16 **ABSTRACT**

36 17 Cancer therapy via redirected lysis mediated by antibodies and antibody-derived
37 18 agents relies on the availability of substantial numbers of sufficiently active immune
38 19 effector cells. To monitor antitumor responses before and during therapy, sensitive
39 20 methods are needed, capable of quantitating specific lysis of target cells. Here we
40 21 present a chip-based single-cell cytometric assay, which uses adherent human target
41 22 cells arrayed in structured micro-fields. Using a fluorescent indicator of cell death and
42 23 time-lapse microscopy in an automated high-throughput mode, we measured specific
43 24 target cell lysis by activated human NK cells, mediated by the therapeutic single
44 25 chain triplebody SPM-2 (33-16-123). This antibody-derived tri-specific fusion protein
45 26 carries binding sites for the myeloid antigens CD33 and CD123 and recruits NK cells
46 27 via a binding site for the Fc-receptor CD16. Specific lysis increased with increasing
47 28 triplebody concentration, and the single-cell assay was validated by direct
48
49
50
51
52
53
54
55
56
57
58
59
60

1
2
3 29 comparison with a standard calcein-release assay. The chip-based approach allowed
4
5 30 measurement of lysis events over 16 hours (compared to 4 hours for the calcein
6
7 31 assay) and required far smaller numbers of primary cells. In addition, dynamic
8
9 32 properties inaccessible to conventional methods provide new details about the
10
11 33 activation of cytolytic effector cells by antibody-derived agents. Thus, the killing rate
12
13 34 exhibited a dose-dependent maximum during the reaction interval. In clinical
14
15 35 applications *ex vivo* monitoring of NK activity of patient's endogenous cells will likely
16
17 36 help to choose appropriate therapy, to detect impaired or recovered NK function, and
18
19 37 possibly to identify rare subsets of cancer cells with particular sensitivity to effector-
20
21 38 cell mediated lysis.
22
23
24
25
26
27
28
29
30

31 **INTRODUCTION**

32
33 41 Several antibody-derived proteins used in cancer therapy function in conjunction
34
35 42 with cytolytic effector cells, such as NK-cells and cytotoxic T-cells (T-CTLs).
36
37 43 Examples are the CD20 antibody Rituximab (Rituxan™) and the CD19-directed
38
39 44 bispecific agent Blinatumomab (Blinicyto™), as well as the bispecific proteins
40
41 45 AMG330 and MGD006, developed for the treatment of Acute Myeloid Leukemia
42
43 46 (AML; ¹⁻⁷). The cytolytic activity of several therapeutic antibodies in the classic IgG
44
45 47 format largely depends on the Fcγ RIII-receptor CD16 present on NK-cells,
46
47 48 monocytes and macrophages⁸⁻¹², while the activity of the mentioned bispecific
48
49 49 agents depends on T-CTLs. Therapeutic use of these agents requires that the patient
50
51 50 harbors the respective effector cells in substantial numbers and in a sufficiently active
52
53 51 state. For AML originating in the bone marrow (BM), this requirement is often not met
54
55 52 during the early stages of treatment. At diagnosis and during the first cycle of
56
57 53 induction therapy of AML patients, NK- and T- cells are usually reduced by about 10-
58
59 54 to 20-fold in numbers relative to a healthy BM, and the remaining cells are
60

1
2
3 55 functionally impaired¹³⁻¹⁶. To determine a suitable therapeutic agent and time point
4
5 56 for the start of treatment, it would therefore help, if investigators could monitor the
6
7 57 capacity of a patient's NK- and/or T-cells to mediate cancer cell lysis in conjunction
8
9 58 with the therapeutic agent. This requires the availability of reliable functional assays
10
11 59 permitting a quantitative assessment of the cytolytic potential of a patient's NK-
12
13 60 and/or T-cells by using only small numbers of these cells, which are available in
14
15 61 limited supply.
16
17
18

19 62 Chromium-51 and Calcein-release assays have been used extensively to
20
21 63 measure cytotoxicity induced by therapeutic agents^{17,18}. However, they cannot be
22
23 64 used for reaction periods in excess of approximately 4 hours due to increasing
24
25 65 spontaneous release of the label from target cells¹⁹. They also do not provide further
26
27 66 information regarding the intrinsic aspects of the investigated cellular interaction. On
28
29 67 the other hand, imaging techniques traditionally offered a more detailed insight into
30
31 68 the interrogated phenomenon, however at low-throughput. This led to the
32
33 69 concomitant use of microscopy to visualize processes that have previously been
34
35 70 hypothesized based on data averaged over large cell populations and produced with
36
37 71 the standard assays²⁰. Nevertheless, time-lapse microscopy has evolved significantly
38
39 72 over the past decade and now permits us to follow the death of individual cells at
40
41 73 high throughput and for observation periods of up to 15 hours and beyond²¹. These
42
43 74 newly developed microscopy-based approaches have uncovered detailed features of
44
45 75 NK physiology and their innate ability to direct lysis of tumor cells, the "natural killing
46
47 76 mode of NK cells". Furthermore, different types of NK cells have been used in these
48
49 77 studies, including both NK-cell lines and primary NK cells activated by IL-2 as well as
50
51 78 unstimulated NK cells isolated from healthy donors. As a result, many different
52
53 79 approaches have been implemented to uncover new aspects of the complex
54
55 80 physiology of NK cells, such as the kinetics of their natural killing mode²² and their
56
57 81 "kinetic boosting" by Fc-engineered antibodies²³. Moreover, the NK population was
58
59
60

1
2
3 82 classified based on migratory behavior and cytotoxic response of individual cells^{24,25}.
4
5 83 Finally, altered NK cell cytotoxicity, migratory behavior and contact dynamics have
6
7 84 been reported between IL-2 stimulated and non-stimulated NK cells²⁶.
8
9

10 85 In oncology Antibody Dependent Cellular Cytotoxicity (ADCC) makes use of
11
12 86 antibodies to enhance the natural killing mode of NK cells^{27,28}. This process more
13
14 87 generally is called “redirected lysis; RDL” when the mediator protein is not an
15
16 88 antibody, but an antibody-derived agent. Although unmodified antibodies in the
17
18 89 classic immunoglobulin (IgG) format have been successful in the treatment of
19
20 90 selected types of cancer, in particular of hematologic malignancies, their broader use
21
22 91 for the treatment of solid tumors is limited. Antibody engineering has led to the
23
24 92 development of more broadly applicable derived proteins²⁹⁻³². Some of these new
25
26 93 molecular formats no longer carry the full antigen-binding-domains of classic IgGs
27
28 94 (Fv-domains) but employ antibody fragments, termed “single-chain Fragment
29
30 95 variables (scFvs)”, as recognition domains. Bispecific tandem diabodies are a class
31
32 96 of recombinant fusion proteins based on scFv-recognition domains, and
33
34 97 Blinatumomab, the prototype of this class of agents, is approved for the treatment of
35
36 98 certain types of lymphomas and leukemias^{3,4}. An extension of the molecular format of
37
38 99 tandem diabodies are the “single-chain tandem triplebodies” (“triplebodies” for
39
40 100 simplicity), which carry two scFv recognition domains for target antigens on the
41
42 101 cancer cell plus an scFv module specific for a trigger molecule on an effector cell,
43
44 102 arranged in tandem in a single polypeptide chain³³⁻³⁵. They can be designed to
45
46 103 bind either two copies of the same target antigen or one copy each of two different
47
48 104 antigens on the surface of the same cancer cell. The latter “dual-targeting” mode of
49
50 105 binding leads to an increased selectivity of cancer cells bearing both antigens in high
51
52 106 combined density^{18,36}. Triplebody SPM-2 (33-16-123) was designed for the
53
54 107 elimination of AML cells. It carries one binding site for CD16 and two binding sites for
55
56 108 the tumor-antigens CD123 and CD33, present on AML cells^{16,34}. Triplebodies can
57
58
59
60

1
2
3 109 bind their target cells either mono-valently with only one of the two target binding
4
5 110 modules, leaving the other module non-engaged, or bi-valently, employing both
6
7 111 target binding modules simultaneously.
8
9

10
11 112 Here we use single-cell cytometry (SCC) to assess the efficiency of SPM-2-
12
13 113 mediated killing of malignant target cells by NK cells in a time-lapse mode. We use a
14
15 114 design where target cells are arranged in arrays of microstructured adhesion sites,
16
17 115 allowing for a facilitated assessment of the fraction of cells specifically lysed by NK
18
19 116 cells, which are added to the assay. We recorded time-lapse movies over a period of
20
21 117 16 hours and followed the action of SPM-2 by the apoptosis marker propidium iodide
22
23 118 (PI). Our main objective was to implement a single-cell assay for time-resolved
24
25 119 studies of the triplebody and NK cell-mediated lysis in accordance with existing
26
27 120 standard assays. The platform presented herein facilitated a dynamic analysis of the
28
29 121 cytotoxic response of the NK cell population triggered by the triplebody. As model
30
31 122 target cells, HEK293.123 cells were used. Our results open the possibility for future
32
33 123 use of the assay to study not only the quality of primary effector cells from human
34
35 124 donors, but also to study mechanistic details of the mode of action of the therapeutic
36
37 125 agent on different subsets of target cells.
38
39
40
41

42 126

43 44 45 127 **RESULTS AND DISCUSSION**

46
47
48
49 128 To quantitate the extent of re-directed lysis of tumor cells by NK cells mediated
50
51 129 by the triplebody SPM-2, we developed a single-cell assay based on fluorescence
52
53 130 microscopy and micro-structured arrays. Arrays of adhesion sites spaced by 60 μ m
54
55 131 were fabricated as previously reported^{37,38} and further described in the Methods
56
57 132 section. The 60 μ m spacing of the adhesion sites was found to be the optimal
58
59 133 distance for generating a single-cell array of the adherent HEK293.123 cells, after
60
134 having tested smaller and larger distances in preliminary tests (data not shown).

1
2
3 135 Triplebody SPM-2 (33-16-123) was synthesized as previously described¹⁶, following
4
5 136 rearrangement, humanization, and stabilization of the DNA sequences of an earlier
6
7 137 prototype of this agent³⁴. Target cells (the established human cell line HEK293.123)
8
9 138 were seeded on the microstructured topas surfaces using ibidi® channel slides.
10
11 139 Figure 1 illustrates the basic experimental imaging platform (Fig. 1A) and a typical
12
13 140 image of a HEK-cell array after addition of NK cells (Fig. 1B). NK cells were derived
14
15 141 from a healthy donor and activated as previously described^{18,39}. Image acquisition
16
17 142 started immediately after NK cell addition. Images were acquired in 12 min intervals
18
19 143 over a time course of 16 hours. The time-lapse sequences were analyzed using
20
21 144 custom-made image-analysis software integrating the fluorescence intensities from
22
23 145 each individual adhesion site at each time-point.
24
25
26
27

28 146 We determined the fraction of specifically lysed cells (% specific lysis),
29
30 147 representing the incremental lysis mediated by NK cells in the presence of the
31
32 148 triplebody SPM-2 over the background of natural killing by NK cells alone according
33
34 149 to the formula given in Methods section. Lysed cells were accounted for based on a
35
36 150 threshold in the PI fluorescence signal. Figure 2 shows the percentage of lysed cells
37
38 151 as a function of triplebody dose. For clarity the percentage of total lysed cells and the
39
40 152 percentage of natural killing by NK-cells are shown together with the calculated
41
42 153 extent of specific lysis.
43
44
45
46

154 **Dose-dependence measurements and comparison with calcein release assay**

47 155 Dose-dependence measurements were also performed with the established
48
49 156 calcein release assay (Figure 2B). For these measurements the effector-to-target cell
50
51 157 (E:T) ratio was kept constant at 2:1 and the concentration of the SPM-2 triplebody
52
53 158 varied from 0 - 100 nM for the SCC assay and from 0 -10 nM for the calcein release
54
55 159 assay. As effector cells immunomagnetically (MACS) purified pre-stimulated NK cells
56
57 160 from the same healthy donor were used. The average percentage of NK cells
58
59 161 (CD56^{bright}CD16^{bright}) after the MACS purification was 83.3 % ± 4.6 %. This
60

1
2
3 162 percentage was taken into account in order to achieve an actual NK-to-target ratio of
4
5 163 2:1 as mentioned above. The total number of target cells analyzed in this set of
6
7 164 measurements is given in Table 1. Over a 16-hour measurement period, a maximum
8
9 165 of about 35% of the cells analyzed were lysed in the SSC assay in the presence of
10
11 166 triplebody SPM-2 (Fig.2A, red open bars). The fraction of specifically lysed cells (%
12
13 167 specific lysis) steadily increased with triplebody concentration and reached a plateau
14
15 168 at about 25 % for concentrations from 1 nM upwards (Fig.2A, red bars). As a
16
17 169 negative control the triplebody SPM-1 (19-16-19) was used, a protein in the same
18
19 170 molecular format as SPM-2 and carrying the same scFv binding site for CD16, but
20
21 171 with specificity for the target antigen CD19, which is absent from the surface of
22
23 172 HEK293.123 cells. In separate experiments with CD19-positive target cells this
24
25 173 control triplebody mediated cytolysis by NK cells³³, but it did not produce specific
26
27 174 lysis of HEK293.123 targets in the SCC assay (Fig.2A, black open bars). The fraction
28
29 175 of specific lysis induced by SPM-2 showed comparable dose-dependence in the SSC
30
31 176 and the calcein-release assays (Fig.2B). In both cases specific lysis reached plateau
32
33 177 values for concentrations from 1 nM upwards, and the shape of the curves was
34
35 178 similar (isometric). The EC50 values (half-maximum effector concentrations; the
36
37 179 concentrations, at which half of the maximum lysis was reached) derived from both
38
39 180 curves were (10.2 ± 8.0) and (12.2 ± 0.1) pM for the calcein and the SCC assays,
40
41 181 respectively. The errors represent the standard deviation computed by statistical
42
43 182 modeling of the two assays (see Methods section). While the EC50 values derived
44
45 183 from both data sets were very similar, the maximum fractions of specifically lysed
46
47 184 cells were (48 ± 2) % for the calcein assay and (25 ± 1) % for the SCC assay. This
48
49 185 difference most likely is explained by the fact that in the calcein assay both effector
50
51 186 and target cells were present in the fluid phase, whereas in the SSC assay the
52
53 187 targets were anchored to the substrate and were therefore less accessible to the
54
55 188 effector cells. In addition, in the SCC assay the density of cells per unit volume was
56
57 189 less than half of the density reached in the calcein assay. However, this quantitative

1
2
3 190 difference in the maximum levels of specific lysis recorded with both assays does not
4
5 191 affect the key conclusion that the SSC assay is validated by this comparison, as it
6
7 192 captured the dose-dependence of the triplebody's lytic potential in the same
8
9 193 qualitative manner as the calcein assay.
10
11

13 194 **Dependence of the extent of cytolysis on the E:T ratio**

15 195 Next we measured the efficiency of lysis as a function of the effector-to-target cell
16
17 196 (E:T) ratio (Fig.3). For measurements of the dependence of this variable on the E:T
18
19 197 ratio, the concentration of the SPM-2 triplebody was kept constant at 1 nM, while the
20
21 198 E:T ratios tested were 0.2:1, 1:1, 2:1 and 5:1. The total number of target cells
22
23 199 analyzed in this set of measurements is given in Table 2. The effector cells used
24
25 200 were MACS-purified NK cells. The mean final percentage of the NK cells
26
27 201 (CD56^{bright}CD16^{bright}) after the enrichment was 90.2 % \pm 3.0%. This percentage was
28
29 202 taken into account in order to reach the actual NK to target cell ratio for each of the
30
31 203 conditions mentioned above. The specifically lysed fraction increased as a function of
32
33 204 the E:T ratio (Fig.3). When the number of effector cells increased the probability for
34
35 205 cell encounters increased too, explaining the increase in lytic events. Furthermore, in
36
37 206 the case of the E:T=5:1 the number of effector cells attacking one single target cell
38
39 207 was also increased. In this case, we observed that more than one effector cells were
40
41 208 able to form a synapse with one specific target cell at the same time. The maximum
42
43 209 extent of specific lysis was achieved at the E:T=5:1 condition.
44
45
46
47
48

49 210 **Dynamic analysis of the lytic events**

50 211 The automated SCC assay allowed us to monitor cellular lysis over a long period
51
52 212 of time with high numeric precision. Focusing on the target cells enabled us to track
53
54 213 the activity of the NK cell population, regarding their cytotoxic activity and how the
55
56 214 SPM-2 agent affected it. In the following, we quantified the killing rate i.e. the number
57
58 215 of lytic events that occurred per hour. This percentage corresponds to the number of
59
60 216 lysed cells versus the total number of target cells analyzed. In Fig.4B, the mean

1
2
3 217 fluorescence intensity of 3 arbitrary single target cells is illustrated, while for one of
4
5 218 these cells the corresponding time-lapse frames of selected time points are
6
7 219 presented (Fig.4A). We determined the individual time points of target cell lysis using
8
9 220 the maximum slope of the fluorescence signal increase as an indicator. From such
10
11 221 data, the cumulative percentage of lysed cells was computed and plotted for 3
12
13 222 different concentrations of SPM-2: 0, 1 and 100 nM (Fig.4C). The variation of the
14
15 223 killing rate over the course of 16 hours for various SPM-2 concentrations and for
16
17 224 constant numbers of NK cells is plotted in Fig.4D. For comparison, the first plot
18
19 225 shows the rate of background lysis rate in the absence of NK cells and the SPM-2
20
21 226 agent (labeled "medium"). When the SPM-2 agent was absent or present in low
22
23 227 concentration, the killing rate of the NK cells was almost constant, 0.5 ± 0.2 target
24
25 228 cells were killed per hour at 0 nM and 1.3 ± 0.5 at 0.01 nM (Fig.4D, 2nd and 3rd panel
26
27 229 from the left). The killing rate increased until a maximum was reached after several
28
29 230 hours into the measurement and then gradually decreased. The maximum rate was
30
31 231 greater for higher concentrations of SPM-2 (50 and 100 nM; last 2 panels to the right
32
33 232 in Fig.4D) than for intermediate concentrations (0.1 to 10 nM; central panels in
34
35 233 Fig.4D), and therefore, the agent clearly influenced the maximum killing rate of the
36
37 234 NK cells. The maximum rate also occurred earlier at high concentrations of the agent
38
39 235 than at lower concentrations (Fig.4D; 2 panels at right). Importantly, the rates of lysis
40
41 236 were elevated in the 1st hour of the reaction (highlighted in yellow in Fig.4D) and
42
43 237 dropped strongly in the 2nd hour for all tested concentrations of the mediator protein,
44
45 238 even without added mediator protein (Fig.4D, 2nd panel from the left). Thereafter the
46
47 239 rates increased until maximum rates were reached between 5-10 hours into the
48
49 240 reaction, and then the rates declined again. The log normal distribution was fitted to
50
51 241 the data points. In all cases, the first data point, indicated in the yellow region
52
53 242 (Fig.4D) was excluded from the fitting, because it consistently was an outlier. We
54
55 243 explain this excessively high lytic rate as being probably owed to the previous
56
57 244 stimulation of the NK cells by long-term culture in the presence of IL-2.

1
2
3 245 NK cells are “ready-to-kill” cells and the most common way to kill is through
4
5 246 perforin/granzyme granule-mediated exocytosis⁴⁰. In this study, LAK (Lymphokine
6
7 247 Activated Killer cells) NK cells, pre-stimulated with IL-2 from a healthy donor, were
8
9 248 used. These cells exhibit greater cytotoxicity due to increased intracellular
10
11 249 concentrations of effector molecules such as perforin and granzymes⁴¹. They form a
12
13 250 synapse with the target cell and then degranulation occurs which leads to apoptotic
14
15 251 death of the target. At the beginning of the measurement the cytosol of the NK cells
16
17 252 is full of granzymes, which then degranulate to lyse the large number of target cells
18
19 253 at the beginning of the measurement. These distinctly large killing rates during the
20
21 254 first hour of the measurement were further boosted by the triplebody in a dose–
22
23 255 dependent manner. Subsequently, the NK cells were exhausted and gradually
24
25 256 resumed their cytotoxic activity by producing again new granzymes. The triplebody
26
27 257 played a role in the early hours of the reaction interval, either in the replenishment
28
29 258 process or the subsequent lytic events or both, because the maximum rates of lysis
30
31 259 were clearly augmented by the triplebody in a dose-dependent manner (Fig.4D). The
32
33 260 observed increase in lytic rates with time suggests an influence of the triplebody on
34
35 261 the speed of replenishment or on other metabolic processes preparing the NK cell for
36
37 262 the next degranulation event and on an acceleration of the cadence of lytic bursts.
38
39 263 Furthermore, the initial increases in the rate during the first few hours of the reaction
40
41 264 may also be a consequence of the lytic events themselves; either the NK cells or the
42
43 265 targets or both may have released soluble mediators (e.g. cytokines and others)
44
45 266 which favored the lytic process in a positive feedback manner (a paracrine loop). At
46
47 267 the same time, the medium was progressively exhausted and cellular debris from
48
49 268 dead target and effector cells accumulated, which must have inhibited the lytic
50
51 269 activity. The system was a closed system in our set-up and the medium was not
52
53 270 renewed. Therefore, these inhibitory influences eventually may have outpaced the
54
55 271 positive feedback mechanisms, an optimum was passed, and beyond this point the
56
57 272 reaction rates began to decline. Moreover, it has been previously shown⁴² that NK
58
59
60

1
2
3 273 cells isolated from healthy donors and stimulated with IL-2 do not have a uniform
4
5 274 cytotoxic activity. In essence a small subset of the NK cells are responsible for the
6
7 275 majority of kills. Finally, taking into consideration that tumor cells can also induce the
8
9 276 apoptosis of IL-2 activated NK cells^{43,44} we propose that the decrease of the reaction
10
11 277 rates after a certain time point most likely was due to a partial apoptosis of the active
12
13 278 cytotoxic subpopulation in combination with the exhaustion of the medium.
14
15
16

17 279 **Natural killing dynamic analysis against non-adherent AML target cells**

18
19
20 280 Many samples of primary cancer cells, especially those derived from hematologic
21
22 281 malignancies, consist of non-adherent cells. To address this matter and to render the
23
24 282 proposed assay suitable for non-adherent cells we developed a second version of
25
26 283 the chip, in which the patterns of squares covered with fibronectin were replaced by
27
28 284 squares covered with an antibody of IgM isotype. To test this variant of our assay, we
29
30 285 measured the natural killing potency of primary NK cells from another healthy donor
31
32 286 for the human AML-derived target cell line MOLM-13.
33
34
35

36 287 A suitable antibody candidate for anchoring MOLM-13 cells to the micro-patterns,
37
38 288 without interfering with the NK cells, is a CD15-specific antibody. The myeloid marker
39
40 289 CD15 is present on the surface of the MOLM-13 cells⁴⁵ but not on the primary NK
41
42 290 cells (Fig.S1). Both IgG1- and IgM-types were tested and MOLM-13 cell arrays of
43
44 291 greater occupancy and greater stability for longer periods of time (up to 24 h) were
45
46 292 achieved with the IgM antibody, probably due to more favorable stereochemical
47
48 293 properties of the IgM relative to the IgG1 isotype. Patterns of squares with 25 μm
49
50 294 side-length were used for the MOLM-13 cell line, because these cells were smaller
51
52 295 than the adherent HEK-cells used so far. As a result, smaller square patterns led to a
53
54 296 greater percentage of single-cell occupied patterns. Even though we could have
55
56 297 chosen smaller distances between the squares for the non-adherent MOLM-13 cells,
57
58 298 we chose to maintain the 60 μm for better comparability with the measurements of
59
60

1
2
3 299 the adherent target cells and to avoid introducing a new variable into the
4
5 300 experimental setup. An array of MOLM-13 cells in the presence of NK cells is shown
6
7 301 in Fig.5A. Size and morphology of MOLM-13 and NK cells are very similar, therefore
8
9 302 MOLM-13 cells were stained with fluorescent tracker dye Green CMFDA to permit
10
11 303 the distinction from the NK cells.
12
13
14

15 304 To test this version of the assay for non-adherent cells we measured the natural
16
17 305 killing of MOLM-13 targets by NK cells alone without addition of a mediating protein.
18
19 306 For the measurements with the non-adherent cells, NK cells were derived from a
20
21 307 second healthy donor and activated by long-term culture in the presence of IL-2 as
22
23 308 previously described^{18,39}. Preparation of the samples, image acquisition and analysis
24
25 309 were performed as described for the measurements with the adherent HEK293.123
26
27 310 cells. The E:T ratio was 2:1 and after a 16-hour measurements period 2.6% of the
28
29 311 cells analyzed were lysed (Fig5.C). This percentage was lower than the average
30
31 312 natural killing observed for the NK cells from the first donor at the same E:T ratio
32
33 313 (8.4%) (Fig.2A), which probably reflects donor-to-donor variability and the different
34
35 314 types of target cells used. Time-lapse frames of an NK cell progressively killing a
36
37 315 MOLM-13 cell are presented in Fig.5B. The variation of the killing rate over the
38
39 316 course of 16 hours for the natural killing of the NK cells measured is presented in
40
41 317 Fig.5D. A slightly greater killing rate during the 1st hour was also observed in this
42
43 318 case and probably reflects the preceding stimulation of the NK cells with IL-2 as was
44
45 319 discussed above.
46
47
48
49
50

51 320

52
53
54 321 Compared with existing methods, single-cell cytometry allows for time-resolved
55
56 322 studies of NK cell activity. Chromium-51 and calcein release assays offer a
57
58 323 statistically valid measurement of cytotoxicity, but they are restricted in duration due to
59
60 324 spontaneous release of the label, and they produce time- and population-averaged

1
2
3 325 data. Flow cytometry and ELISPOT assays offer single-cell data for large number of
4
5 326 cells, but also only for at a single time point. Moreover, they measure cytotoxicity in
6
7 327 an indirect manner, as with flow cytometry usually target cells that have survived are
8
9 328 counted, while in ELISPOT assays usually IFN- γ secretion or degranulation of the
10
11 329 effector cells is measured^{46,47}. The SCC assay presented here fills the gap between
12
13 330 these two different approaches of measuring cytotoxicity. SCC is capable of following
14
15 331 the progression of NK cytotoxic activity over an extended duration of 16 hours. Due
16
17 332 to spatial ordering of the target cells, image analysis is feasible with limited
18
19 333 computational means generating data that contain full information on the time course
20
21 334 of killing events relevant to therapeutic applications.
22
23
24
25

26 335 To better understand the mode of action of novel therapeutics based on the
27
28 336 recruitment of effector cells and the functional properties of the effector cells
29
30 337 involved, it is essential to have the ability to study also the dynamics of these
31
32 338 processes. Additional studies will likely produce suggestions for optimal dosing and
33
34 339 administration schedules in clinical applications. Time-lapse methods are promising
35
36 340 in this regard, since meta-analysis can be extended to the use of additional markers
37
38 341 including biomarkers of therapy success, disease progression and impending
39
40 342 relapse, and because they lend themselves to further automatization.
41
42
43

44 343 An additional advantage of single cell assays is that they generate reliable data
45
46 344 with substantially smaller numbers of effector cells. For an SCC assay typically only
47
48 345 2×10^4 NK cells are needed per measurement point, 5-times fewer than the $>10^5$ cells
49
50 346 needed for each measurement point in a calcein release assay. Patient-derived NK
51
52 347 cells are a scarce resource, in particular to monitor disease status and therapy
53
54 348 outcome for AML patients. Further miniaturization of the new method is possible, so
55
56 349 that reliable measurements will likely become possible with as few as 5 000 - 10 000
57
58 350 NK cells. Furthermore, patterned arrays provide uniform micro-environments and
59
60 351 spacing of target cells and hence potentially improve the standardization of cell-cell

1
2
3 352 encounters. Hence, chip-based single cell assays are potentially valuable for clinical
4
5 353 monitoring of the patients NK response and for the choice of personalized treatment
6
7 354 for individual AML patients. They can also be applied to T-CTL as effector cells in
8
9
10 355 combination with corresponding triplebodies and with other antibody-derived proteins
11
12 356 recruiting T-cells as cytolytic effectors^{4-7,48}.

13
14
15 357 Assays employing spatially arrayed target cells can also be useful to study
16
17 358 questions regarding the timing in cell-cell recognition and immune response, such as
18
19 359 for example the "memory" effect described for NK cells²². In the experiments
20
21 360 presented here the full potential of the dual-targeting triplebody SPM-2 has not yet
22
23 361 been analyzed. Here we have so far only used the CD123-binding site of this agent.
24
25 362 In the future the effect of simultaneous engagement of both binding sites by one copy
26
27 363 each of CD33 and CD123 on the lytic activity of NK cells can be studied. Dual-
28
29 364 targeting renders the SPM-2 agent particularly promising for the therapy of AML
30
31 365 because virtually all patients expressed either one or the other of the two antigens⁴⁹.
32
33 366 Indeed, in cell culture cytotoxicity assays with primary cells from a broad range of AML
34
35 367 patients with different subtypes of AML and with a standard batch of NK cells from an
36
37 368 unrelated healthy donor, all samples showed very effective lysis⁵⁰. This is an
38
39 369 unusually high degree of responsiveness, considering that the response rate to the
40
41 370 best antibody-derived agent available so far for the treatment of AML (MylotargTM 51)
42
43 371 was in the range of 40 % for blasts from patients with different subtypes of AML⁵².
44
45 372 Even blasts from patients with AML subtypes that typically show a poor response to
46
47 373 conventional chemotherapy were lysed efficiently by SPM-2 plus NK cells⁵⁰.
48
49 374 Moreover, the pair of CD33 plus CD123 is highly expressed on AML leukemia stem
50
51 375 cells (AML-LSCs) but far less on normal hematopoietic stem cells (HSCs; ⁵²⁻⁵⁴).
52
53 376 Therefore, a therapeutic window appears to exist, which may permit a preferential
54
55 377 elimination of the AML-LSCs over the normal HSCs of the patient and a
56
57 378 reconstitution of the patient's hematopoietic system after the end of therapy from the
58
59
60

1
2
3 379 patient's own HSCs, without the need for an allogeneic or autologous stem cell
4
5 380 transplantation. If this could be achieved in the future, then this result would
6
7 381 constitute major progress in the therapy of AML. Therefore, in the future it is
8
9 382 important to study in detail not only how a patient's autologous NK cells in
10
11 383 conjunction with this agent lyse the patient's bulk AML blasts, but also whether and
12
13 384 how they lyse subsets of blasts progressively closer and closer to the leukemia
14
15 385 initiating cells (LICs) and relapse initiating MRD cells, which are likely to be
16
17 386 encompassed in the CD34^{pos}CD38^{neg}CD123^{high} compartment of BM and peripheral
18
19 387 blood cells, which comprises between 0.01 and 67% of all malignant cells for
20
21 388 different AML patients⁵⁵. To this end cytolysis assays with rare subsets of patient-
22
23 389 derived AML cells and NK- or T cells are required, which will be available in small
24
25 390 numbers only. Finally, agents targeting the same pair of antigens, but recruiting T-
26
27 391 cells as cytolytic effectors are also under development⁵⁶, and similar experiments as
28
29 392 those outlined above will also need to be performed with the corresponding T-cell-
30
31 393 recruiting agents in order to find the best suited agent for individual patients in the
32
33 394 sense of a personalized medicine. Developments are well under way that
34
35 395 personalized medicine will clearly become more prevalent in the future. Time-
36
37 396 resolved SSC assays are promising means to further investigate the capabilities of
38
39 397 Fc engineered antibodies and other bi- and tri-specific antibody-derived agents such
40
41 398 as the triplebodies described here for enhanced target cell lysis. They therefore offer
42
43 399 the potential to assist treatment decisions and monitoring of treatment success in
44
45 400 cancer therapy.
46
47
48
49
50

51
52 401

53
54
55 402 **EXPERIMENTAL**

56
57
58 403 **Cell culture**
59
60

1
2
3 404 Human Embryonic Kindey 293 cells (HEK 293), obtained from the American Type
4
5 405 Cell Culture Collection (ATCC, Manassas, VA, USA), were transfected with cDNA
6
7 406 expression constructs for human CD123 and sublimes were selected, which stably
8
9
10 407 expressed CD123 over many passages in culture. The subline employed here has
11
12 408 been in culture for several years and stably expresses approx. 360 000 copies of
13
14 409 CD123 per cell on the surface⁵⁷. It was cultured in RPMI 1640 medium (Biochrom;
15
16 410 Merck Millipore, Berlin, Germany) supplemented with 10% (vol/vol) Fetal Bovine
17
18 411 Serum (FBS; Gibco®, Life Technologies GmbH, Darmstadt, Germany) and 400
19
20 412 µg/ml Geneticin Selective Antibiotic G418 Sulfate (Roth, Karlsruhe, Germany).
21
22
23 413 MOLM-13 cells were cultured in RPMI 1640 medium supplemented with 10%
24
25 414 (vol/vol) FBS.

26
27
28 415 **Ex vivo expansion of MNCs from healthy donors in the presence of IL-2 and**
29
30 416 **immunomagnetic enrichment of NK cells**

31
32 417 Mononuclear cells (MNCs) from peripheral blood (PBMCs) were expanded *ex*
33
34 418 *vivo* in RPMI medium containing Interleukin-2 (IL-2) plus 5% (vol/vol) human serum
35
36 419 (Life Technologies) for 20 days as described^{18,39} and were then frozen in aliquots for
37
38 420 subsequent use. Prior to use in cytotoxicity experiments, the cells were thawed and
39
40 421 cultured overnight in RPMI medium containing 5% (vol/vol) human serum plus 50
41
42 422 units/ml of penicillin and 50 µg/ml of streptomycin (PS; Life Technologies)
43
44 423 respectively, but no additional IL-2. NK cells were then enriched by negative
45
46 424 selection using the human NK Cell Isolation Kit (Miltenyi Biotec; Cat. No. 130-092-
47
48 425 657; Bergisch Gladbach, Germany) according to the provider's instructions. The
49
50 426 enriched batches contained 83-90% of CD56^{bright} CD16^{bright} NK cells.

51
52
53
54 427

55
56
57
58 428 **Surface patterning**

59 429 Protein-coated arrays were prepared on polymer coverslips for 6-channel sticky
60 430 slides (ibidi GmbH, Munich, Germany). First, coverslips were treated selectively with

1
2
3 431 oxygen plasma (40 W for 3 min; Femto, Diener Electronic GmbH + Co. KG,
4
5 432 Ebhausen, Germany). Selectivity was achieved using a polydimethylsiloxane (PDMS)
6
7 433 stamp (cast from a master produced by photolithography) as a mask. The area
8
9 434 exposed to plasma was passivated with PLL(20k)-g(3.5)-PEG(2k) (SuSoS AG;
10
11 435 Dübendorf, Switzerland) at 1 mg/ml in aqueous buffer (10mM HEPES pH 7.4 and
12
13 436 150 mM NaCl). Then the PDMS stamp was removed and the remaining hydrophobic
14
15 437 areas (squares 30 × 30 µm) were exposed to fibronectin (50 µg/ml; YO Proteins AB,
16
17 438 Huddinge, Sweden) for 1 hour. Finally, channels were rinsed thoroughly with PBS
18
19 439 and the slides were stored at 4 °C for a maximum of 5 days. Before cell seeding,
20
21 440 PBS was exchanged with culture medium (RPMI with 10% (vol/vol) FBS) and kept for
22
23 441 1 hour at 37 °C.
24
25
26
27

28 442 The same procedure was followed for the antibody-coated arrays with the
29
30 443 following alterations: arrays were prepared on uncoated 8-well µ-slides (ibidi GmbH,
31
32 444 Munich, Germany). After treatment with plasma, the PDMS stamp was removed and
33
34 445 the remaining hydrophobic areas (squares 25 x 25 µm) were exposed to purified anti-
35
36 446 human CD15 (SSEA-1) antibody (15µg/ml; BioLegend®, San Diego, CA USA) for 1
37
38 447 hour at room temperature.
39
40
41

42 448 **Time-resolved fluorescence microscopy**

43 449 *Sample preparation*

44
45 450 For the fluorescence microscopy measurements 6-channel/8-well slides were
46
47 451 used (ibidi GmbH) with protein-coated arrays. HEK293.123 cells were added to the
48
49 452 channels (10 000 cells per channel) and incubated at 37 °C, in culture medium for
50
51 453 approx. 4 hours, until the cells were deposited in an array. MOLM-13 cells were
52
53 454 stained in 1µM CellTracker™ Green CMFDA dye (Thermo Fischer Scientific,
54
55 455 Waltham, MA USA) for 15 min in serum-free media in 37°C, followed by 1h of
56
57 456 recovery in complete media. Then stained cells were seeded into the wells (10 000
58
59
60

1
2
3 457 cells per well), and after 2 hours the culture medium was exchanged to Leibovitz's
4
5 458 L15 medium with GlutaMAX (Gibco®, Life Technologies) supplemented with 10%
6
7 459 (vol/vol) FBS. Meanwhile, final solutions with the appropriate number of MACS
8
9 460 enriched NK cells and the desired concentration of the SPM-2 triplebody or control
10
11 461 agents were prepared and added to the channels/wells. A trypan blue exclusion test
12
13 462 of the NK cells was performed immediately before the preparation of the final
14
15 463 solutions.
16
17
18
19
20 464

21
22 465 Imaging was performed under an inverted Nikon Ti eclipse microscope with a
23
24 466 motorized stage, a Plan Achromat 4x/0.2 N.A. objective, an Andor Clara-E
25
26 467 camera, and a Lumencor SOLA LED lamp. For detection of PI fluorescence a filter
27
28 468 cube with 540/25nm (excitation) and 630/60nm (emission) filters was used. For the
29
30 469 stained MOLM-13 cells a filter cube with 470/40nm (excitation) and 525/50nm
31
32 470 (emission) filters was used. Images were taken with constant exposure times of 10
33
34 471 and 300 ms in the brightfield and the PI/Green CMFDA channels respectively at 12-
35
36 472 min intervals for 16 hours. A pre-determined X-Y position list was used for the
37
38 473 automated time-lapse recording of 84 positions for each measurement. During the
39
40 474 recording samples were kept at a constant temperature of 37 °C using an ibidi
41
42 475 heating system (ibidi GmbH).
43
44
45
46
47

48 476 **Image and data analysis**

49 477 Raw images were pre-processed with ImageJ (<http://imagej.nih.gov/ij/>). Using an
50
51 478 in-house plugin, *Microwell Analysis*, an orthogonal grid was aligned over cells and
52
53 479 single-cell occupied grid positions were selected. The mean intensities over the
54
55 480 selected positions of the grid were extracted and exported to a data file. Custom
56
57 481 Matlab scripts (MATLAB version R2014b Natick, Massachusetts: The MathWorks
58
59 482 Inc., 2014) were employed to quantify the number of dead target cells and to find
60

1
2
3 483 their lysis time-points based on the maximum slope of the signal increase in the PI
4
5 484 channel. In the representative set of data, a threshold was chosen as a maximum
6
7 485 value that can separate the weakest signal of a dead target cell from the background
8
9
10 486 signals e.g. from healthy cells. Further analysis confirmed that the threshold was at
11
12 487 least 4 times higher than the background fluorescence intensity of the healthy cells in
13
14 488 the PI channel. Specific lysis was calculated as:

$$specific\ lysis\% = \left(\frac{fraction\ lysed\ with\ SPM2 - fraction\ lysed\ without\ SPM2}{total\ cells - spontaneous\ cell\ deaths} \right) \times 100\%$$

15
16
17
18
19
20
21
22 489

23
24
25 490

26
27
28 491 **Redirected Lysis (RDL) assays using Calcein release**

29 492 Target cells HEK293.123 were pre-labeled with Calcein AM (Life Technologies)
30
31
32 493 and mixed with MACS-purified NK cells in RPMI 1640 GlutaMAX medium
33
34 494 supplemented with 10% (vol/vol) FBS at E:T = 2:1. SPM-2 triplebody was added at
35
36 495 the desired concentration to a 200 μ L reaction volume in round-bottom 96-well
37
38 496 plates. Reactions were incubated at 37 $^{\circ}$ C with 5% CO₂ for 4 hours. Calcein release
39
40 497 was quantitated by measuring the fluorescence intensity (relative light units, RLU) in
41
42 498 the supernatant using a fluorimeter/ELISA plate reader at 485/535 nm. Maximum
43
44 499 lysis was achieved by addition of 50 μ L of a solution containing 10 % Triton X-100 in
45
46 500 RPMI 1640 GlutaMAX medium supplemented with 10 % (vol/vol) FBS and 1 %
47
48 501 (vol/vol) PS. Specific cellular cytotoxicity was expressed as overall lysis minus the
49
50 502 background of spontaneous lysis mediated by the NK cells alone, in the absence of
51
52 503 added antibody-reagents. Specific lysis was evaluated by the formula:

$$specific\ lysis\% = \left(\frac{RLU(sample) - RLU(background)}{RLU(maximal\ lysis) - RLU(background)} \right) \times 100\%$$

53
54
55
56
57
58
59
60 504

1
2
3 505
4
5
6

7 **506 Statistical analysis**

8 507 In the case of the single-cell cytometry (SCC) assay we hypothesized that data
9
10 508 follow the binomial distribution and error bars were calculated with a confidence level
11
12
13 509 of 95 %.

14
15
16 510 **Statistical modeling of the calcein assay and single cell assay results**

17
18
19 511 *Statistical modeling of the single cell assay*

20 512 Five different conditions were interrogated (0, 0.01, 0.1, 1, and 10nM). For every
21
22 513 condition we considered the number of dead cells and the number of cells in total.
23
24 514 The problem at hand was to calculate the EC50 and its confidence interval of the
25
26 515 dose response curve with measurements in these 5 conditions/concentrations. The
27
28 516 concentrations correspond to the independent variable, and the ratio of dead
29
30 517 cells/total cells corresponds to the response variable of the model (curve). From here
31
32 518 on the log10 of the concentrations was used.

33
34
35
36
37 519 We hypothesized that the killing events in every condition can be modeled using
38
39 520 a binomial distribution. The metrics of the binomial distributions were calculated using
40
41 521 the binofit() function in Matlab. Then, these binomial distributions were sampled with
42
43 522 replacement to generate 1000 random measurements (in terms of dead cells) per
44
45 523 condition (concentration). From this random sampled number of dead cells we
46
47 524 subtracted the number of dead cells observed for the 0 nM condition and divided by
48
49 525 the corresponding number of total cells, having subtracted the number of
50
51 526 spontaneous cell death events. This number corresponds to the specific killing ratio.
52
53 527 Dose response curves in the form of a sigmoid curve were fitted for every set of
54
55 528 random killing ratios, yielding 1000 random sampled dose response curves. The fit of
56
57 529 the sigmoid curves was performed using the nlinfit() function in Matlab. From the
58
59 530 sigmoid curves the parameters corresponding to the EC50 values were extracted
60

1
2
3 531 and averaged across all 1000 random samplings yielding a mean value and a
4
5 532 standard deviation.
6
7
8

9 533 *Statistical modeling of the calcein assay*

10 534 Here, we considered the specific lysis ratio measured directly using the calcein
11
12 535 assay. The mean specific lysis ratios and corresponding standard deviations for the 5
13
14 536 conditions discussed above were used as an input to this analysis. We hypothesized
15
16 537 that the lysis ratios in every condition can be modeled by using a normal distribution.
17
18 538 We used these distributions in similar fashion as above to generate random
19
20 539 measurements in terms of lysis ratios for every condition and to fit sigmoid curves to
21
22 540 model dose response. From the sigmoid curves the terms corresponding to the EC50
23
24 541 were extracted and averaged across all random samplings to yield a mean and a
25
26 542 standard deviation.
27
28
29
30

31 543
32
33

34 544 **CONCLUSIONS**

35
36
37 545 Single cell arrays combined with time-resolved fluorescence microscopy were
38
39 546 used to study the interaction of primary human NK cells with human target cells
40
41 547 mediated by triplebody SPM-2, an antibody-derived protein, which recruits NK cells
42
43 548 for target cell lysis. The arrayed pattern of target cells allowed for highly efficient and
44
45 549 automated counting of lytic events under standardized conditions. Lysis depended on
46
47 550 the dose of the agent and the E:T ratio in a manner typical for standard cytotoxicity
48
49 551 assays, and therefore this new assay was validated relative to existing standard
50
51 552 procedures (calcein release assay). Use of the new SCC assay revealed so far
52
53 553 unreported changes in the killing rate over long-term reaction periods (16 hours).
54
55 554 Finally, a variation of the assay employing surface-coated antibodies demonstrated
56
57 555 the feasibility to array non-adherent target cells in the chip-based single-cell
58
59 556 cytometric assay. The proposed platform facilitates testing the susceptibility of many
60

1
2
3 557 tumor-derived cell types to lysis by NK cells with or without an added mediator
4
5 558 protein and can become a useful tool for the design of personalized therapies.
6
7

8
9 559

10
11
12
13 560 **ACKNOWLEDGEMENTS**

14
15 561 Financial support by the Deutsche Forschungsgemeinschaft within the
16
17 562 Excellence Graduate School Quantitative BioSciences (QBM) and the program
18
19 563 project grant (Sonderforschungsbereich) SFB 1032 (project B01) is gratefully
20
21 564 acknowledged. We thank Prof. Karl Peter Hopfner, LMU University Munich;
22
23 565 Germany, for kind gifts of purified SPM-2 protein, and Dr. Christoph Stein,
24
25 566 Fraunhofer Institute, Aachen, Germany, for the HEK293.123 cells. We are grateful to
26
27 567 Max Albert for wafer and chip fabrication, and to Peter J. Röttgermann for
28
29 568 microscopic pictures of the fibronectin-coated arrays.
30
31

32
33 569

34
35
36
37
38 570 **DISCLOSURE OF POTENTIAL CONFLICT OF INTEREST**

39 571 The authors declare no conflict of interest.
40
41
42

43 572

44
45
46
47 573 **REFERENCES**

- 48
49 574
50 575 1. L. Weiner, J. Murray, and C. Shuptrine, *Cell*, 2012, **148**.
51
52 576 2. P. McLaughlin, A. J. Grillo-López, B. K. Link, R. Levy, M. S. Czuczman, M.
53 577 E. Williams, M. R. Heyman, I. Bence-Bruckler, C. A. White, F. Cabanillas, V. Jain,
54 578 A. D. Ho, J. Lister, K. Wey, D. Shen, and B. K. Dallaire, *J. Clin. Oncol.*, 1998, **16**,
55 579 2825–33.
56 580 3. T. Dreier, G. Lorenczewski, C. Brandl, P. Hoffmann, U. Syring, F. Hanakam,
57 581 P. Kufer, G. Riethmuller, R. Bargou, and P. A. Baeuerle, *Int. J. Cancer*, 2002, **100**,
58 582 690–7.
59 583 4. R. Bargou, E. Leo, G. Zugmaier, M. Klingler, M. Goebeler, S. Knop, R.
584 584 Noppeney, A. Viardot, G. Hess, M. Schuler, H. Einsele, C. Brandl, A. Wolf, P.

- 1
2
3 585 Kirchinger, P. Klappers, M. Schmidt, G. Riethmüller, C. Reinhardt, P. Baeuerle, and
4 586 P. Kufer, *Science (New York, N.Y.)*, 2008, **321**, 974–7.
5 587 5. M. Aigner, J. Feulner, S. Schaffer, R. Kischel, P. Kufer, K. Schneider, A.
6 588 Henn, B. Rattel, M. Friedrich, P. A. Baeuerle, A. Mackensen, and S. W. Krause,
7 589 *Leukemia*, 2013, **27**, 1107–15.
8 590 6. M. Friedrich, A. Henn, T. Raum, M. Bajtus, K. Matthes, L. Hendrich, J. Wahl,
9 591 P. Hoffmann, R. Kischel, M. Kvesic, J. W. Slootstra, P. A. Baeuerle, P. Kufer, and B.
10 592 Rattel, *Mol. Cancer Ther.*, 2014, **13**, 1549–57.
11 593 7. C. go. identifier NCT02152956, .
12 594 8. T. Takai, M. Li, D. Sylvestre, R. Clynes, and J. V. Ravetch, *Cell*, 1994, **76**,
13 595 519–29.
14 596 9. G. Cartron, L. Dacheux, G. Salles, P. Solal-Celigny, P. Bardos, P. Colombat,
15 597 and H. Watier, *Blood*, 2002, **99**, 754–8.
16 598 10. W.-K. K. Weng and R. Levy, *J. Clin. Oncol.*, 2003, **21**, 3940–7.
17 599 11. M. Albanesi, D. A. Mancardi, L. E. Macdonald, B. Iannascoli, L. Zitvogel, A.
18 600 J. Murphy, M. Daëron, J. H. Leusen, and P. Bruhns, *J. Immunol.*, 2012, **189**, 5513–7.
19 601 12. F. Nimmerjahn and J. V. Ravetch, *Nat. Rev. Immunol.*, 2008, **8**, 34–47.
20 602 13. R. T. T. Costello, S. Sivori, E. Marcenaro, M. Lafage-Pochitaloff, M.-J. J.
21 603 Mozziconacci, D. Reviron, J.-A. A. Gastaut, D. Pende, D. Olive, and A. Moretta,
22 604 *Blood*, 2002, **99**, 3661–7.
23 605 14. C. Fauriat, S. Just-Landi, F. Mallet, C. Arnoulet, D. Sainty, D. Olive, and R.
24 606 T. Costello, *Blood*, 2007, **109**, 323–30.
25 607 15. E. Lion, Y. Willemen, Z. N. Berneman, V. F. Van Tendeloo, and E. L. Smits,
26 608 *Leukemia*, 2012, **26**, 2019–26.
27 609 16. T. Braciak, S. Wildenhain, C. Roskopf, I. Schubert, G. Fey, U. Jacob, K.-P.
28 610 Hopfner, and F. Oduncu, *Journal of Translational Medicine*, 2013, **11**, 289.
29 611 17. K. T. Brunner, J. Mael, J. C. Cerottini, and B. Chapuis, *Immunology*, 1968,
30 612 **14**, 181–96.
31 613 18. I. Schubert, D. Saul, S. Nowecki, A. Mackensen, G. H. Fey, and F. S. Oduncu,
32 614 *MAbs*, 2014, **6**, 286–96.
33 615 19. D. L. Nelson, C. C. Kurman, and D. E. Serbousek, *Curr Protoc Immunol*,
34 616 2001, **Chapter 7**, Unit 7.27.
35 617 20. R. Bhat and C. Watzl, *PLoS ONE*, 2007, **2**.
36 618 21. J. Albeck, J. Burke, B. Aldridge, M. Zhang, D. Lauffenburger, and P. Sorger,
37 619 *Molecular Cell*, 2008, **30**.
38 620 22. P. Choi and T. Mitchison, *Proceedings of the National Academy of Sciences*,
39 621 2013, **110**, 6488–6493.
40 622 23. G. Romain, V. Senyukov, N. Rey-Villamizar, A. Merouane, W. Kelton, I.
41 623 Liadi, A. Mahendra, W. Charab, G. Georgiou, B. Roysam, D. A. Lee, and N.
42 624 Varadarajan, *Blood*, 2014, **124**, 3241–9.
43 625 24. E. Forslund, K. Guldevall, P. E. Olofsson, T. Frisk, A. E. Christakou, M.
44 626 Wiklund, and B. Onfelt, *Front Immunol*, 2012, **3**, 300.
45 627 25. Unknown, .
46 628 26. P. E. Olofsson, E. Forslund, B. Vanherberghen, K. Chechet, O. Mickelin, A.
47 629 R. Ahlin, T. Everhorn, and B. Onfelt, *Front Immunol*, 2014, **5**, 80.
48 630 27. C. Shuptrine, R. Surana, and L. Weiner, *Seminars in cancer biology*, 2012, **22**,
49 631 3–13.
50 632 28. A. Scott, J. Wolchok, and L. Old, *Nature Reviews Cancer*, 2012, **12**, 278–287.
51 633 29. P. J. Carter, *Nat. Rev. Immunol.*, 2006, **6**, 343–57.
52 634 30. R. E. Kontermann, *MAbs*, 2012, **4**, 182–97.

- 1
2
3 635 31. R. Kontermann and U. Brinkmann, *Drug Discovery Today*, 2015.
4 636 32. C. Spiess, Q. Zhai, and P. J. Carter, *Mol. Immunol.*, 2015.
5 637 33. C. Kellner, J. Bruenke, J. Stieglmaier, M. Schwemmlein, M. Schwenkert, H.
6 638 Singer, K. Mentz, M. Peipp, P. Lang, F. Oduncu, B. Stockmeyer, and G. H. Fey, *J.*
7 639 *Immunother.*, 2008, **31**, 871–84.
8 640 34. M. Kügler, C. Stein, C. Kellner, K. Mentz, D. Saul, M. Schwenkert, I.
9 641 Schubert, H. Singer, F. Oduncu, B. Stockmeyer, A. Mackensen, and G. H. Fey, *Br. J.*
10 642 *Haematol.*, 2010, **150**, 574–86.
11 643 35. H. Singer, C. Kellner, H. Lanig, M. Aigner, B. Stockmeyer, F. Oduncu, M.
12 644 Schwemmlein, C. Stein, K. Mentz, A. Mackensen, and G. H. Fey, *J. Immunother.*,
13 645 2010, **33**, 599–608.
14 646 36. J. M. Rowe and B. Löwenberg, *Blood*, 2013, **121**, 4838–41.
15 647 37. P. J. Röttgermann, A. P. Alberola, and J. O. Rädler, *Soft Matter*, 2014, **10**,
16 648 2397–404.
17 649 38. M. Ferizi, C. Leonhardt, C. Meggle, M. Aneja, C. Rudolph, C. Plank, and J.
18 650 Rädler, *Lab on a chip*, 2015, **15**, 3561–71.
19 651 39. E. Alici, T. Sutlu, B. Björkstrand, M. Gilljam, B. Stellan, H. Nahi, H. C.
20 652 Quezada, G. Gahrton, H.-G. G. Ljunggren, and M. S. Dilber, *Blood*, 2008, **111**, 3155–
21 653 62.
22 654 40. M. J. Smyth, E. Cretney, J. M. Kelly, J. A. Westwood, S. E. Street, H. Yagita,
23 655 K. Takeda, S. L. van Dommelen, M. A. Degli-Esposti, and Y. Hayakawa, *Mol.*
24 656 *Immunol.*, 2005, **42**, 501–10.
25 657 41. M. Cheng, Y. Chen, W. Xiao, R. Sun, and Z. Tian, *Cellular & Molecular*
26 658 *Immunology*, 2013, **10**, 230–252.
27 659 42. B. Vanherberghen, P. E. Olofsson, E. Forslund, M. Sternberg-Simon, M. A.
28 660 Khorshidi, S. Pacouret, K. Guldevall, M. Enqvist, K.-J. J. Malmberg, R. Mehr, and B.
29 661 Önfelt, *Blood*, 2013, **121**, 1326–34.
30 662 43. A. Poggi, A.-M. Massaro, S. Negrini, P. Contini, and M. Zocchi, *The Journal*
31 663 *of Immunology*, 2005, **174**, 2653–2660.
32 664 44. G. M. Spaggiari, P. Contini, A. Dondero, R. Carosio, F. Puppo, F. Indiveri, M.
33 665 R. Zocchi, and A. Poggi, *Blood*, 2002, **100**, 4098–107.
34 666 45. Matsuo, MacLeod, Uphoff, Drexler, Nishizaki, Katayama, Kimura, Fujii,
35 667 Omoto, Harada, and Orita, *Leukemia*, 1997, **11**, -.
36 668 46. A. Malyguine, S. Strobl, K. Dunham, M. Shurin, and T. Sayers, *Cells*, 2012, **1**.
37 669 47. E. Ranieri, I. Popescu, and M. Gigante, *Methods Mol. Biol.*, 2014, **1186**, 75–
38 670 86.
39 671 48. C. C. Roskopf, C. B. Schiller, T. A. Braciak, S. Kobold, I. A. Schubert, G. H.
40 672 Fey, K.-P. P. Hopfner, and F. S. Oduncu, *Oncotarget*, 2014, **5**, 6466–83.
41 673 49. Ehninger, Kramer, Röllig, Thiede, Bornhäuser, von Bonin, Wermke,
42 674 Feldmann, Bachmann, Ehninger, and Oelschlägel, *Blood Cancer Journal*, 2014, **4**,
43 675 e218.
44 676 50. T. A. Braciak, C. C. Roskopf, S. Wildenhain, N. Fenn, C. Schiller, I. A.
45 677 Schubert, U. Jacob, A. Honegger, C. Krupka, M. Subklewe, K. Spiekermann, K.-P.
46 678 Hopfner, G. H. Fey, M. Aigner, S. Krause, A. Machensen, and F. S. Oduncu,
47 679 *Oncotarget*, in press.
48 680 51. A. Burnett, M. Wetzler, and B. Löwenberg, *J. Clin. Oncol.*, 2011, **29**, 487–94.
49 681 52. C. T. Jordan, D. Upchurch, S. J. Szilvassy, M. L. Guzman, D. S. Howard, A.
50 682 L. Pettigrew, T. Meyerrose, R. Rossi, B. Grimes, D. A. Rizzieri, S. M. Luger, and G.
51 683 L. Phillips, *Leukemia*, 2000, **14**, 1777–84.
52 684 53. A. W. Hauswirth, S. Florian, D. Printz, K. Sotlar, M.-T. T. Krauth, G. Fritsch,

- 1
2
3 685 G.-H. H. Schernthaner, V. Wacheck, E. Selzer, W. R. Sperr, and P. Valent, *Eur. J.*
4 686 *Clin. Invest.*, 2007, **37**, 73–82.
5 687 54. R. B. Walter, F. R. Appelbaum, E. H. Estey, and I. D. Bernstein, *Blood*, 2012,
6 688 **119**, 6198–208.
7 689 55. F. Vergez, A. S. Green, J. Tamburini, J.-E. E. Sarry, B. Gaillard, P. Cornillet-
8 690 Lefebvre, M. Pannetier, A. Neyret, N. Chapuis, N. Ifrah, F. Dreyfus, S. Manenti, C.
9 691 Demur, E. Delabesse, C. Lacombe, P. Mayeux, D. Bouscary, C. Recher, and V.
10 692 Bardet, *Haematologica*, 2011, **96**, 1792–8.
11 693 56. C. Arndt, A. Feldmann, M. von Bonin, M. Cartellieri, E.-M. M. Ewen, S.
12 694 Koristka, I. Michalk, S. Stamova, N. Berndt, A. Gocht, M. Bornhäuser, G. Ehninger,
13 695 M. Schmitz, and M. Bachmann, *Leukemia*, 2014, **28**, 59–69.
14 696 57. C. Stein, C. Kellner, M. Kügler, N. Reiff, K. Mentz, M. Schwenkert, B.
15 697 Stockmeyer, A. Mackensen, and G. Fey, *British Journal of Haematology*, 2010, **148**,
16 698 879–889.
17 699
18 700
19 701
20
21
22
23
24
25 702
26
27
28
29
30
31
32
33
34
35
36
37
38
39
40
41
42
43
44
45
46
47
48
49
50
51
52
53
54
55
56
57
58
59
60

1
2
3
4
5
6
7
8
9
10
11
12
13
14
15
16
17
18
19
20
21
22
23
24
25
26
27
28
29
30
31
32
33
34
35
36
37
38
39
40
41
42
43
44
45
46
47
48
49
50
51
52
53
54
55
56
57
58
59
60

703 **Figure 1: Experimental set-up of the single-cell cytometry (SCC) assay.**

704 Chemically modified patterned surfaces (arrays) were prepared on 6-channel
705 microscope slides (A). Protein-coated arrays were generated by plasma-induced
706 patterning. B: Squares with a side-length of 30 μm were coated with fibronectin (here
707 fibronectin labeled with Alexa Fluor 488) and the backfilling (black) area with
708 PLL(20k)-g(3.5)-PEG(2k) (PEG(2)). Each channel on the carrier surface, shown in
709 (A), contained 4400 adhesive squares for cell attachment. In (B) a part of an
710 overview microscopic scan of one coated channel of the slide is shown. C: Arrays of
711 adherent HEK293.123 target cells were prepared on the chemically modified
712 surfaces (surfaces seeded with cells have adhesive squares with unlabeled
713 fibronectin). NK cells were added and squares occupied by single target cells
714 (framed in blue) were selected and tracked in a time-lapse mode. NK cells were
715 identified cinematographically by their size and motility. The distance between the
716 squares was 60 μm in our experiments, but arrays with different spacing can be
717 produced. D: The cell-impermeable red fluorescent marker PI (propidium iodide) was
718 used to identify dead cells. Overlay of brightfield and PI emission is presented for the
719 first and last frame of a measurement. E: The mean fluorescence intensity of 40 cells
720 over time is plotted (in the presence of 10nM SPM-2 triplebody). Each track ("fate
721 plot") represents the fluorescence intensity of one cell in the PI channel. Tracks
722 exceeding an intensity threshold (defined by a supervised selection process as
723 described under Methods) represent lysed cells. Two exemplary time-courses of two
724 target cells that were lysed are highlighted in red.

725

726 **Figure 2: Validation of the SCC assay by direct comparison with the bulk assay.**

727 A: Data obtained with the SCC assay. Red open bars: percentage of dead target
728 cells relative to the total number of target cells analyzed ("overall lysis"). Red filled
729 bars: percentage of specific lysis induced by SPM-2 after subtraction of natural killing

1
2
3 730 by NK cells alone (the numbers shown for 0 nM concentration). Black open bars:
4
5 731 overall lysis produced by addition of control triplebody SPM-1 (19-16-19), a triplebody
6
7 732 in the same molecular format as SPM-2, but recognizing the target antigen CD19,
8
9 733 which is absent from HEK293.123 cells. This control was not performed for 50 and
10
11 734 100 nM concentrations of the control protein. Medium control: without added NK cells
12
13 735 and triplebodies; this control measures the extent of spontaneous death of target
14
15 736 cells over the measurement interval. The averaged value of all the dose-dependent
16
17 737 measurements is shown. (B) Comparison of data obtained with the SCC assay (red
18
19 738 circles) over a 16 hour measurement and the bulk assay (calcein release assay; blue
20
21 739 circles) over a 4 hour period. Data points of the calcein assay represent the mean
22
23 740 value of the percentage of specific lysis averaged over triplicate reaction wells on the
24
25 741 same microtiter plate, and error bars represent the SEM (standard error of the
26
27 742 mean). Effector cells were MACS-purified NK cells from a healthy donor, pre-
28
29 743 stimulated with IL-2 (LAK cells), and seeded at an E:T ratio of 2:1.

30
31
32
33
34
35 744

36
37
38 745 **Figure 3: Dependence of specific lysis measured with the SCC assay on the E:T**
39
40 746 **ratio.** Lysis induced over a range of different Effector to Target (E:T) cell ratios by
41
42 747 SPM-2 at a 1 nM saturating concentration. Data points are fitted to an exponential
43
44 748 curve. Effector cells were MACS-purified NK cells from a healthy donor, pre-
45
46 749 stimulated with IL-2 (LAK cells).

47
48
49
50 750

51
52
53 751 **Figure 4: Dynamic analysis of lytic events with the SCC assay.** (A) Time-lapse
54
55 752 images of an exemplary target cell being killed by an NK cell (arrow). The
56
57 753 progressively increased PI fluorescence intensity reflects progressive nuclear
58
59 754 membrane disintegration (irreversible apoptosis). (B) PI fluorescence intensity of 3
60
755 exemplary target cells over the course of 16 hours, including the cell shown in (A)

1
2
3 756 (red curve). Raw intensities were fitted with the Hill Equation. (C) Cumulative
4
5 757 percentage of lysed target cells for 3 different concentrations of SPM-2: 0, 1 and 100
6
7 758 nM. Data points were fitted with the sigmoid function. (D) Killing rate as a function of
8
9
10 759 time for increasing concentrations of SPM-2 by a constant number of NK cells. The
11
12 760 left panel (“medium”) shows the dynamic of spontaneous cell death events, in the
13
14 761 absence of NK cells. Data points were fitted with a log normal distribution curve. Data
15
16 762 points for the first hour of the reaction (highlighted in yellow) represent natural killing
17
18 763 by the NK cells but not specific lysis mediated by the triplebody. These events also
19
20 764 occurred in the absence of added triplebody (2nd panel from the left), and were
21
22
23 765 therefore excluded from the fitting.
24
25
26 766

27
28
29 767 **Figure 5: Variation of the SCC assay adapted to non-adherent target cells.**

30
31 768 Arrays of antibody coated square patterns were generated with the same procedure
32
33 769 as the fibronectin arrays, by substituting fibronectin with an anti-human CD15
34
35 770 antibody. Arrays of stained MOLM-13 cells (CellTracker™ Green CMFDA) were
36
37 771 prepared on the chemically modified surfaces and then NK cells (unstained) were
38
39 772 added (A). (B) Time-lapse images of an exemplary MOLM-13 target cell (green)
40
41 773 being killed by an NK cell (unstained). The progressively increased PI fluorescence
42
43 774 intensity reflects progressive nuclear membrane disintegration (irreversible
44
45 775 apoptosis). (C) Data obtained with the SCC assay showing the natural killing potency
46
47 776 of NK cells against MOLM-13 cells. The bars represent the percentage of dead target
48
49 777 cells relative to the total number of target cells analyzed. (D) Dynamic analysis of the
50
51 778 natural killing mode of NK cells against the MOLM-13 target cells. The right panel
52
53 779 (“medium”) shows the dynamic of spontaneous cell death events, in the absence of
54
55 780 NK cells.
56
57
58
59
60

781

1
2
3 782 **Table 1:** Total number of target cells analyzed in dose-dependence
4
5 783 measurements
6
7
8
9 784

nM	SP	Control
	M-2	triplebody
0	30	465
	99	
0.0	16	303
	48	
0.1	18	507
	88	
1	34	524
	82	
10	32	344
	54	
50	15	-
	28	
100	13	-
	64	
me dium	30	489
	75	

785

786

787 **Table 2:** Total number of target cells analyzed in measurements of the
 788 dependence on the E:T ratio

789

E:T	1	0
	nM	nM
0.2:	1	1
1	061	300
1:1	9	8
	92	15
2:1	3	7
	482	44
5:1	1	8
	309	67
me	1	1
dium	909	909

790

791 **Table 3:** Total number of target cells analyzed in measurements with the non-
 792 adherent cells

E:T	=	mediu
2:1		m

1
2
3
4
5
6
7
8
9
10
11
12
13
14
15
16
17
18
19
20
21
22
23
24
25
26
27
28
29
30
31
32
33
34
35
36
37
38
39
40
41
42
43
44
45
46
47
48
49
50
51
52
53
54
55
56
57
58
59
60

1775	2276
------	------

793

794

795

1
2
3 796
4
5
6
7 797
8
9
10
11
12
13
14
15
16
17
18
19
20
21
22
23
24
25
26
27
28
29
30
31
32
33
34
35
36
37
38
39
40
41
42
43
44
45
46
47
48
49
50
51
52
53
54
55
56
57
58
59
60

ABSTRACT	2	
INTRODUCTION	3	
Calcein release assays, cell-to-cell comparison with calcein release assays and dependence of the extent of cytolysis on the E:T ratio	8	8
Dynamic analysis of the lytic events	10	
Natural killing dynamic analysis against non-adherent AML target cells	12	
EXPERIMENTAL	17	
Cell culture	17	
Ex vivo expansion of MNCs from healthy donors in the presence of IL-2 and immunomagnetic enrichment of NK cells	17	17
Surface patterning	18	
Time-resolved fluorescence microscopy	19	
Sample preparation	19	
Image and data analysis	20	
Adirected Lysis (RDL) assays using Calcein release	20	20
Statistical analysis	21	
Statistical modeling of the calcein assay and single cell assay results	21	21
Statistical modeling of the single cell assay	21	
Statistical modeling of the calcein assay	22	
ACKNOWLEDGEMENTS	23	
CLOSURE OF POTENTIAL CONFLICT OF INTEREST	23	23
REFERENCES	24	

Development of a chip-based platform for dynamic analysis of adherent and non-adherent target cell cytolysis by Natural Killer cells.

Figure 1

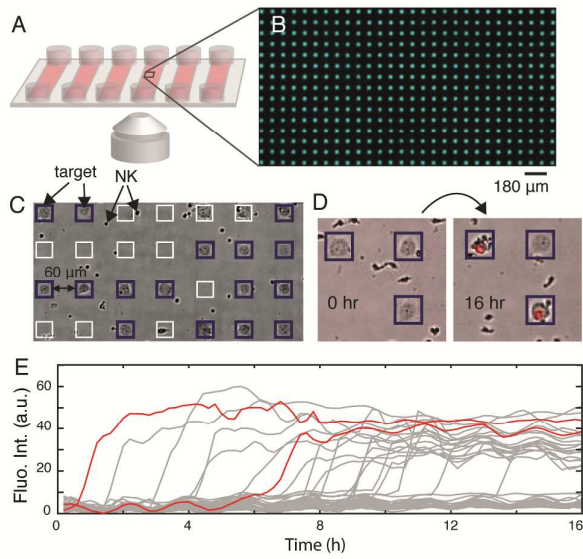
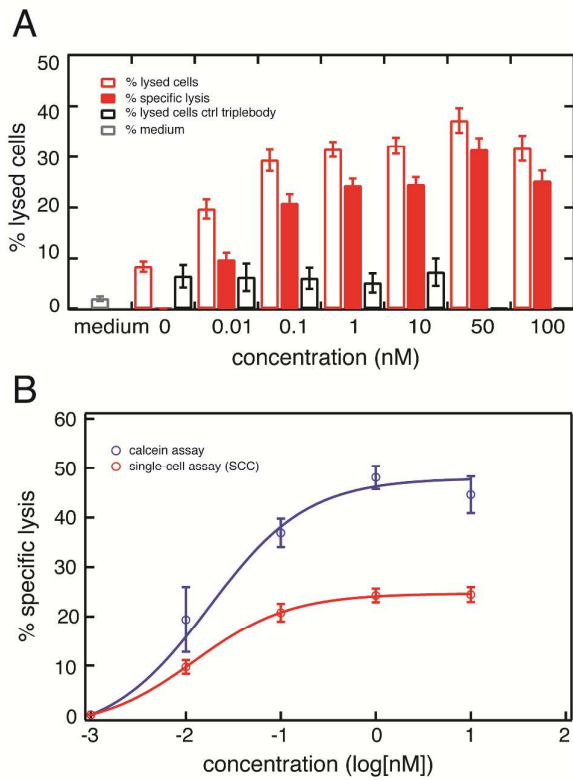


Figure 2



1
2
3
4
5
6
7
8
9
10
11
12
13
14
15
16
17
18
19
20
21
22
23
24
25
26
27
28
29
30
31
32
33
34
35
36
37
38
39
40
41
42
43
44
45
46
47
48
49
50
51
52
53
54
55
56
57
58
59
60

1
2
3
4
5
6
7
8
9
10
11
12
13
14
15
16
17
18
19
20
21
22
23
24
25
26
27
28
29
30
31
32
33
34
35
36
37
38
39
40
41
42
43
44
45
46
47
48
49
50
51
52
53
54
55
56
57
58
59
60

Figure 3

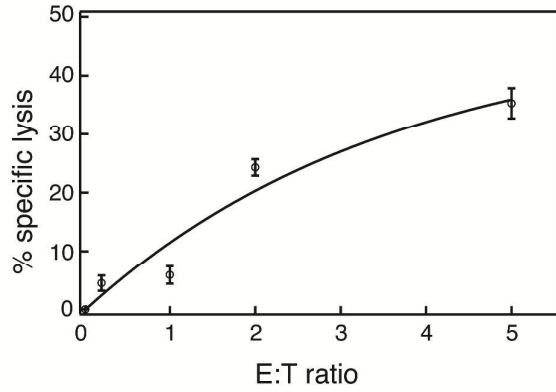
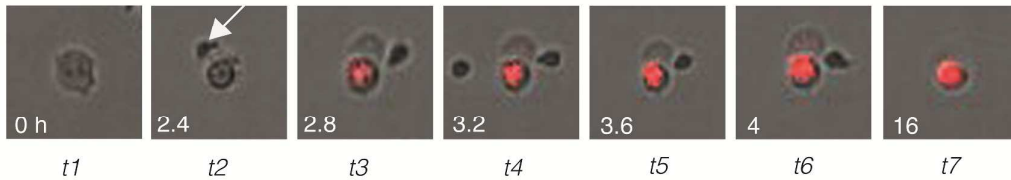
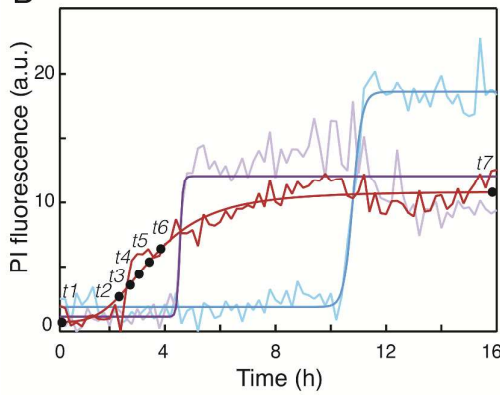


Figure 4

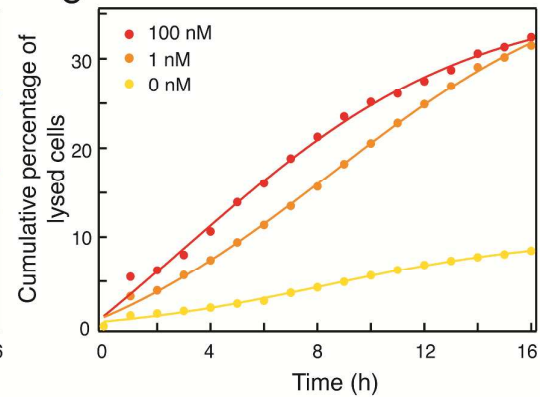
A



B



C



D

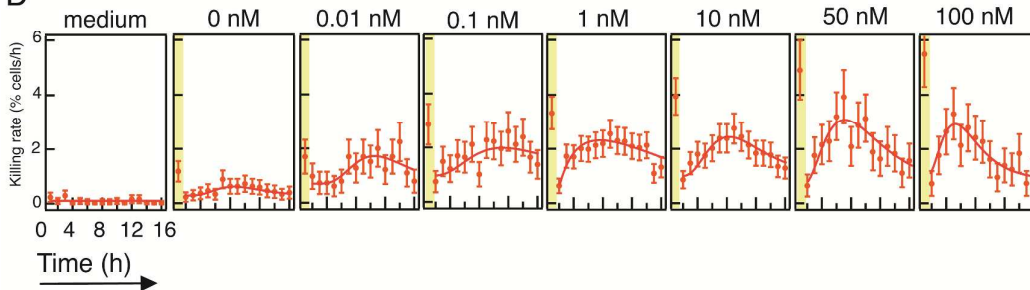
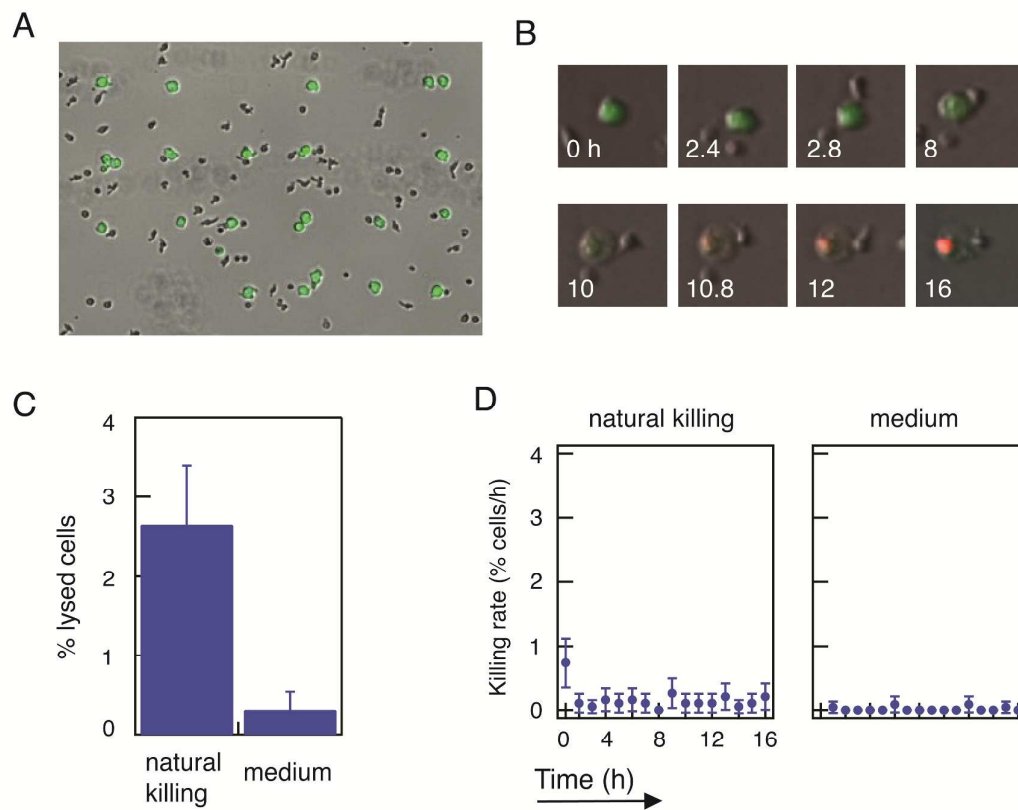


Figure 5



1
2
3
4
5
6
7
8
9
10
11
12
13
14
15
16
17
18
19
20
21
22
23
24
25
26
27
28
29
30
31
32
33
34
35
36
37
38
39
40
41
42
43
44
45
46
47
48
49
50
51
52
53
54
55
56
57
58
59
60